

Document Version

Final published version

Licence

CC BY

Citation (APA)

Sreejith, K. P., Zeiher, N., Sluijs, P., Venkatesh, V., Mathiazhagan, G., Vasudevan, R., Ziar, H., & Smets, A. H. M. (2026). Screening hotspots in flexible thin-film amorphous silicon foils using current injection dependent electroluminescence imaging. *Solar Energy Materials and Solar Cells*, 300, Article 114282. <https://doi.org/10.1016/j.solmat.2026.114282>

Important note

To cite this publication, please use the final published version (if applicable). Please check the document version above.

Copyright

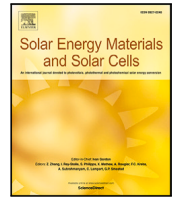
In case the licence states "Dutch Copyright Act (Article 25fa)", this publication was made available Green Open Access via the TU Delft Institutional Repository pursuant to Dutch Copyright Act (Article 25fa, the Taverne amendment). This provision does not affect copyright ownership. Unless copyright is transferred by contract or statute, it remains with the copyright holder.

Sharing and reuse

Other than for strictly personal use, it is not permitted to download, forward or distribute the text or part of it, without the consent of the author(s) and/or copyright holder(s), unless the work is under an open content license such as Creative Commons.

Takedown policy

Please contact us and provide details if you believe this document breaches copyrights. We will remove access to the work immediately and investigate your claim.



Screening hotspots in flexible thin-film amorphous silicon foils using current injection dependent electroluminescence imaging

K.P. Sreejith^{a,*}, Niklas Zeiher^a, Peer Sluijs^a, Vijay Venkatesh^a, Gayathri Mathiazhagan^b, Ravi Vasudevan^b, Hesam Ziar^a, Arno H.M. Smets^{a,*}

^a Photovoltaic Materials and Devices (PVMD), Delft University of Technology, 2628CD Delft, The Netherlands

^b HyET Solar B.V., Westervoortsedijk 71K, 6827 AV Arnhem, The Netherlands

ARTICLE INFO

Keywords:

Thin-film silicon solar cells
Hotspot endurance testing
Electroluminescence imaging
Reliability of flexible solar panels

ABSTRACT

This work introduces a method for screening potential hotspots in monolithic interconnected thin-film silicon modules using injection-dependent electroluminescence (EL) imaging. The fraction of dark area of the cell in the low- and high-injection EL images, respectively, is used to extract the severity and localization information associated with a defect. For the first time, a factor, namely, severity-to-localization (SL), is introduced for each defect as the ratio of severity to localization. Further, defects are broadly classified as A, B, AB, and C modes. Mode A and Mode B are severe, where the former is a distributed defect across the cell, and the latter is a localized defect. In contrast, Mode C is a localized trivial defect. The severe defects that are neither entirely distributed within the cell area nor localized are classified as Mode AB. The SL factor values associated with A, B, AB, and C modes are ≈ 1 , > 4 , between 1 and 4, and ≈ 1 , respectively. Furthermore, the potential of four modes of defects for hotspot formation is tested following the IEC61215 standard. The hotspot endurance test results reveal that high SL factor defects, such as Mode B, always lead to hotspots, and low SL factor defects, such as Mode A and C, do not produce distinguishable hotspots. Similarly, Mode AB with a higher SL formed clear hotspots, and with a lower SL factor (< 1.5) never formed hotspots. The proposed method applies to all thin-film technologies with monolithic interconnects and is, therefore, expected to gain significant attention.

1. Introduction

In recent decades, photovoltaic (PV) technology has emerged as the most suitable alternative to conventional fossil-based energy technologies to reduce the carbon footprint for climate change mitigation purposes. PV systems are projected to become the largest installed renewable energy source worldwide, surpassing wind and hydro by 2030 with a cumulative installation of nearly 6 TW [1]. Integration of PV panels to all possible sites, such as buildings (BIPV), vehicles (VIPV), floating structures, corrugated surfaces, transportation hubs, etc., can significantly accelerate efforts towards decarbonizing the energy infrastructure [2]. State-of-the-art crystalline silicon technology mostly employs glass-backsheet encapsulation and glass-glass encapsulation, respectively, for monofacial and bifacial designs [3–5]. The PV glass used for encapsulation is very rigid and contributes to nearly 70% of the module weight for monofacial design itself, which limits its application in BIPV, VIPV, corrugated surface, and transportation hub-related installations [6,7]. Roll-to-roll processed thin-film PV modules with polymer encapsulation are ideal candidates for installation sites where weight, rigidity, and glare from glass are a concern [8–10].

However, in addition to bulk defects, roll-to-roll processing and laser scribing used for monolithic interconnection can introduce a large areal density of defects in thin-film PV panels [11,12]. A higher density of shunts, cracks, and defects not only reduces the energy yield but also imposes reliability issues such as hotspot failures in the field [13–18].

Hotspots are the hotter regions of a solar cell or a PV module. A hotspot occurs when the short circuit current (I_{SC}) of a cell in the string is lower than the module operating current due to partial shading or soiling [19,20]. In such a case, the shaded cell is forced to operate in reverse bias, and the excess power generated by other cells is dissipated as heat across the shaded cell [21–23]. Moreover, with the presence of shunt paths such as cell cracks, hotspot heating can be localized and severe with temperature raising to 150°C for non-uniform shading [13,16]. Prolonged hotspots in conventional crystalline silicon modules lead to failure modes such as glass and cell breakage, soldering degradation, and encapsulant discoloration [24,25]. Bypass diodes are commonly used across the substrings of crystalline silicon panels to reduce energy loss and prevent adverse effects of hotspots [26–28]. In contrast, the extent and impact of hotspot heating in flexible thin-film

* Corresponding authors.

E-mail addresses: S.KoorthedathPullayikody@tudelft.nl (K.P. Sreejith), A.H.M.Smets@tudelft.nl (A.H.M. Smets).

<https://doi.org/10.1016/j.solmat.2026.114282>

Received 14 May 2025; Received in revised form 5 March 2026; Accepted 5 March 2026

Available online 6 March 2026

0927-0248/© 2026 The Authors. Published by Elsevier B.V. This is an open access article under the CC BY license (<http://creativecommons.org/licenses/by/4.0/>).

modules can be severe, especially for monolithic interconnect designs where the integration of bypass diodes is not possible. Several studies reported that thin film panels in reference to crystalline silicon panels performed better under shading and exhibited higher tolerance to hotspots because of their cell arrangement and geometry [29–33]. However, defect-induced localized heating may still pose reliability risks, such as the melting of polymer encapsulants. The IEC61215 testing standard includes a separate procedure for hotspot endurance testing (HSET) of series-connected thin amorphous silicon PV modules [34]. The procedure for HSET consists of two main steps: identification of worst-case shading scenarios (WCSS) and prolonged light soaking. WCSS refers to finding the combination of solar cells with the least I_{SC} at shading. Subsequently, the worst performing combination of cells is shaded, and the rest of the module is illuminated for a prolonged time of 1 h at elevated temperature under short circuit conditions [34]. Conditions such as elevated temperature, short-circuiting the panel, and shading of entire cells are included in the testing protocols to account for extreme conditions that are unlikely in field operations. The HSET pass or fail criteria are based on visual inspection for any new defects, such as discolouration and burn marks [34]. Interestingly, the IEC61215 testing procedures do not screen for defects. Also, to the best of the authors' knowledge, a detailed study on classifying the defects for potential hotspots has not been reported yet, especially for monolithic interconnected thin-film modules.

Current–voltage (I–V) tracing, infrared (IR) imaging, dark lock-in thermography (DLIT), and electroluminescence (EL) imaging are some of the commonly employed techniques to analyse the quality of finished PV panels. Forward bias I–V tracing provides performance parameter values such as open circuit voltage (V_{OC}), fill factor (FF), I_{SC} , shunt resistance (R_{Sh}) and series resistance (R_S). Reverse I–V sweeps can also provide information on the leakage currents and ohmic behaviour of the shunts [35–37]. However, acquiring the I–V data of each cell in a module is a cumbersome process, especially for monolithic interconnected modules. In addition, the I–V tracing does not provide spatial information. Although IR imaging is a simple, non-invasive, and fast scanning technique used to identify damaged panels and cells, especially for large-scale installations, it often produces poor contrast images. It also does not provide information on the underlying cause [38–41]. DLIT is a heat dissipation-based technique that is used to generate shunt maps of both cells and modules with reverse biasing [42–44]. However, application of DLIT can be invasive for polymer encapsulated and monolithic interconnected thin-film PV due to the localized heating effects induced by severe shunts. In contrast, EL imaging is a non-destructive technique that provides high-resolution spatial maps of defects [45–47]. EL imaging is applied in crystalline silicon cells and modules to characterize a wide range of reliability issues such as optical degradation [48,49], R_S -related problems [50, 51], and shunting problems [52,53]. The industry uses EL imaging as a quality assurance technique for screening defects such as microcracks in wafer-based solar cells. Limited literature is also available on the application of EL images to characterize defects in monolithic interconnected thin-film modules [54–59]. These studies suggest that EL imaging is an effective and reliable method for identifying various defects and degradations in PV modules.

This work presents a method for screening potential hotspots in thin amorphous silicon modules. EL images captured for two current injections are used to classify the defects in four different modes in general. The classification is based on the severity and spatial distribution of information extracted from the high and low current injection EL images. Subsequent HSET results reveal that severe and localized defects can form strong hotspots while shading. We also demonstrate that the extent of hotspot heating can be qualitatively predicted based on a factor estimated from the luminescence patterns associated with each mode of defects in the two injection EL images. This method can be employed as a quality check for screening the defects responsible for field failures in monolithic interconnected amorphous silicon modules. The proposed technique is also expected to gain significant attraction among different PV manufacturers, as it can be applied to any thin-film technology.

2. Experimental details

2.1. Injection dependent EL imaging

A schematic diagram of the EL set-up used in this study is shown in Fig. 1(a). EL setup consists primarily of a programmable power supply, a camera with appropriate filters, a PV module under investigation, and a computer. The DC power supply used in this study is from dataTech GmbH. Two current levels of standard testing conditions (STC) I_{SC} and 20% of STC I_{SC} , respectively, referred to as high and low current injections, are used to generate spatial EL maps. The EL camera assembly consists of a Nikon D7200 with a 28 mm f/1.8G lens and an IR filter. The integration durations used to capture high- and low-injection EL images were 2 min and 30 min, respectively. In addition, the captured greyscale EL images were processed in Matlab for defect classification and analysis.

The simplified electrical equivalent circuit of a PV cell (module) during EL imaging inside a dark room is shown in Fig. 1(b). Here, V_{EL} and V_D , respectively, represent the voltage applied during EL imaging and the voltage available to the characteristic diode of the PV cell. R_S and R_{Sh} , respectively, represent the series and shunt resistances of the cell. Similarly, I_{EL} , I_{Sh} , and I_D indicate the current injected into the PV module, the current sink by R_{Sh} , and the current available to the characteristic diode component of the solar cell to generate radiative signals. As indicated in Fig. 1(b), I_D leads to EL emissions due to band-to-band recombination and hence is also dependent on the recombination characteristics of the diode [60]. The expression for EL intensity (ϕ_{EL}) can be written as [61];

$$\phi_{EL} = C e^{\frac{V_D}{V_T}} \quad (1)$$

where C and V_T , respectively, are the calibration constant and thermal voltage across the diode. Depending on the type and the process from which it originated, the presence of defects results in an increase in diode saturation current density, or an increase in R_S , or a decrease in R_{Sh} , which subsequently reduces ϕ_{EL} [62]. Hence, recombination-related, R_S -related defects (e.g., metallization issues such as finger breaks) and shunt-related defects (e.g., cracks and laser scribing issues) can be seen in EL images, especially for high-current injection conditions [62–64].

When a low current of 20% STC I_{SC} is injected into a PV module with severe shunts, the shunt itself sinks a significant fraction of the injected current, and only a small fraction of the current will be available across the characteristic diode to generate radiative signals. In contrast, the entire injected current will be available to the characteristic diode in the case of cells with high R_{Sh} values. Hence, low-injection EL images provide good contrast in luminescence between shunted and non-shunted cells, with the former appearing entirely dark or significantly less luminescent. In addition, R_S -related defects are not prominently visible in low-injection EL images due to only a negligible difference in voltage across R_S and V_D . However, at high-injection, irrespective of the large shunts, there will be sufficient current available to the characteristic diode on the other parts of the solar cells to produce radiative signals. Only regions close to shunts emerge as dark in EL images, and non-shunted cells appear uniformly luminescent. This suggests that high-injection EL imaging can provide insights into the distribution and position of the defects. In addition, R_S -related and recombination-related defects can also be distinguished from shunts, as they are more prominently seen only in high-injection EL images. In summary, it can be seen that the severity of the shunts can be extracted from the low-injection EL imaging, and the distributed or lumped nature of the shunts can be identified from the high-injection EL imaging. Following this argument, a severity to localization (SL) factor is introduced for the first time to screen the defects that can lead to hotspot formation during shading. Although high- and low-injection EL imaging is employed for the detection of defects such as microcracks

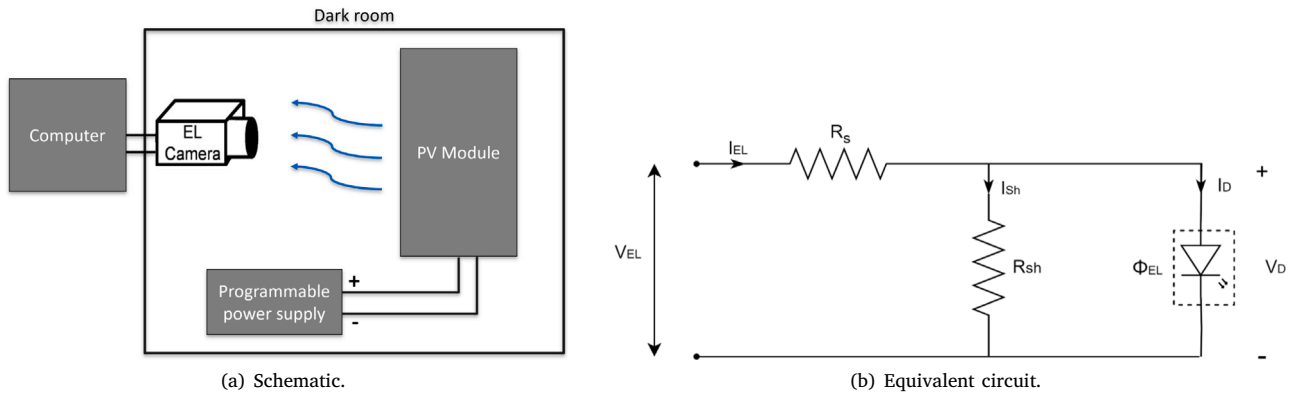


Fig. 1. Depicts the (a) schematic and (b) simplified equivalent circuit diagram of EL imaging of a PV module under dark conditions.

and UV-induced degradation, none have used the combination of high- and low-injection EL images to classify defects based on both their location and severity. The SL factor is defined based on the luminescence pattern at low- and high-injection EL imaging as;

$$SL = \frac{\text{Fraction of dark area of the cell at low injection EL image}}{\text{Fraction of dark area of the cell at high injection EL image}} \quad (2)$$

The value of the SL factor can be as low as 1 for distributed and not-severe defects and as high as >10 for very localized and severe defects.

2.2. Process flow

The process flow used in this work is shown in Fig. 2. The thin amorphous silicon (a-Si) single junction PV modules used in this study consist of 28 cells with an individual cell area of $30 \text{ cm} \times 1 \text{ cm}$. The cells are laser-scribed, monolithic interconnected and exhibit divergent EL signals. Since the study involves the characterization of defects, PV modules that have divergent defects are intentionally chosen from a large batch of modules, and these modules are used for experiments. Initially, the PV modules were visually inspected thoroughly for any defects, such as discolouration or burn marks. Subsequently, high- and low-injection EL images were captured. The predictor defects seen in the EL imaging are then broadly classified as four modes based on the luminescence pattern observed in the high- and low-injection. During HSET, the cell containing the defect and an adjacent cell are shaded together using a custom-made opaque mask (that cover two cells), and the modules were illuminated for an hour at 50°C at short-circuit conditions, as recommended in the IEC61215 certification norms. Throughout the HSET, the temperature of the stage in which solar panels were mounted was regulated using chiller to avoid any additional thermal stress. The IEC61215 testing standard endorses an illumination intensity in the range of $1000 \pm 100 \text{ W m}^{-2}$, while the illumination intensity used in the study was 720 W m^{-2} . The spectral energy of the metal halide lamp used is mostly distributed over the wavelength range of 400 nm to 750 nm , ideal for harvesting maximum I_{SC} in thin-film PV technologies. In this regard, the full area illumination (without shading any combination of solar cells) I_{SC} of modules measured each time prior to the HSET was nearly 10% higher than the STC I_{SC} for all modules. Furthermore, after 60 min of HSET, the hotter regions (hotspots) in the shaded area are captured through an IR camera. The Fluke Ti32 infrared camera was used to capture the thermal images without removing the opaque mask and ammeter connection. The emissivity of the thermal camera was set to 70%. Finally, the PV modules are visually inspected again for additional burn marks or discolouration in reference to the initial visual inspection.

3. Results and discussion

3.1. Classification of defects

Based on the severity and location information extracted from the low-injection and high-injection EL images, the defects are broadly classified as Mode A, Mode B, Mode AB, and Mode C. The schematic representations of the luminescence associated with each mode of defects at low- and high-current injection are summarized in Table 1. Except for Mode C, all three other modes of defects show low luminescence across the entire solar cell area at low-injection. This implies that these defects sink a significant fraction of the injected current and can be classified as severe. However, in the case of Mode C defects, only a small area near the defect location is seen as dark, suggesting that there is still enough current available to the other regions of the solar cells to generate radiative signals. Hence, this category (Mode C) of defects has relatively mild shunting effects in reference to the other three modes.

In contrast to low-injection EL images, only Mode A defects exhibit low luminescence throughout the entire cell area in high-injection EL images. This indicates that Mode A is either a distributed defect that spreads across the cell area or has multiple point defects within the cell. The exact nature of the distribution and locations of Mode A defects are hard to estimate from high-injection EL images because both uniformly distributed and multiple severe point defects can lead to a uniformly dark luminescence pattern across the entire cell area at high-injection. Compared to a low-injection EL image, Mode B defects exhibit low luminescence only in a localized region, and Mode C defects appear similar in high-injection EL images. This suggests that Mode B and Mode C defects are very localized as the injected current results in luminescence across the cell area except at the neighbourhood region of these defects. As the name indicates, Mode AB defects have the characteristics of both Mode A and Mode B defects, where they are neither very localized nor completely distributed in the cell area. For instance, the localization associated with the cells can vary, as shown in Table 1. The Mode AB defect present at cell 5 is much more localized (has close characteristics of Mode B), and the Mode AB defect at cell 10 exhibits a distributed nature like Mode A defects. A localization factor of 20% is used to distinguish between a Mode B and Mode AB defect at high-injection. If a strong defect exhibits a low luminescence level below 20% of the total cell area at high-injection, they are classified as Mode B; otherwise, it belongs to Mode AB.

The SL factor associated with different defect modes is also listed in Table 1. Mode B defects have the highest SL factor of >4 as they are not only severe but also very locally distributed. The SL factor estimated for some mode B defects was as high as >10 . A higher SL factor in Mode B implies that the defects are very localized. Irrespective of the different characteristics in terms of severity and distribution, the SL factor associated with Mode A and Mode C is nearly unity as they

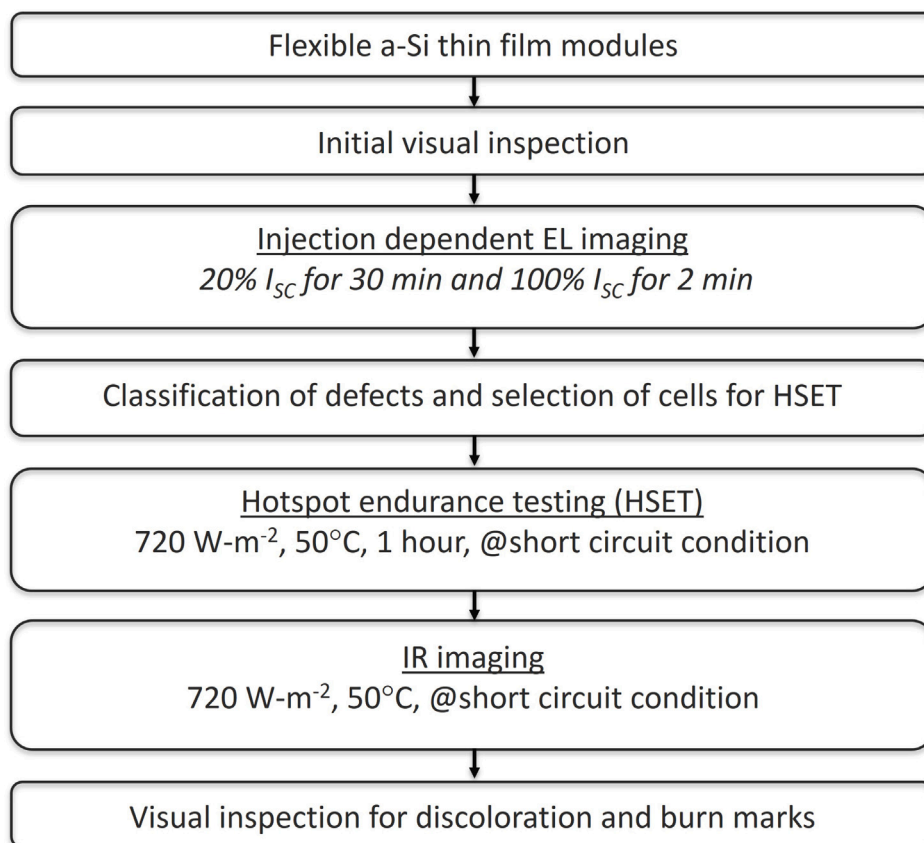


Fig. 2. Process steps used for the HSET of amorphous silicon PV modules.

exhibit similar luminescence patterns in both high- and low-injection EL images. Mode AB defects have varied SL factors typically in the range of 1 to 4, mainly due to the variation in luminescence pattern seen in high-injection EL images. For the examples in Table 1, the mode AB defect shown in cell 5 has an SL factor of nearly 3, whereas the Mode AB at cell 10 has an SL factor close to 1.5. Mode AB defects with SL factor >3 exhibit the close-range characteristics of a Mode B defect whereas Mode AB defect with SL factor <1.5 has the characteristics of Mode A defects. Importantly, the definition of the SL factor opens the possibility of applying this classification method to modules of different dimensions.

The low- and high-injection EL images of a representative thin-film silicon PV module with different defect modes after processing in MATLAB are shown in Fig. 3. The different modes discussed in Table 1 are also marked in these EL images. It can be seen that solar cells containing Mode A (cell number 6), Mode AB (cell number 12), and Mode B (cell number 14) show nearly no luminescence throughout the cell area at low-injection (see Fig. 3(a)). Whereas in the high-injection EL image (Fig. 3(b)), the cell containing Mode A shows very low luminescence throughout the cell area, the defect in Mode AB results in a dark spot for nearly 30% and Mode B exhibits a very localized dark spot at the bottom of the cell. The Mode C defect in cell 28 shows a very localized dark spot at the same region for high- and low-injection EL images. Magnified high-injection EL images of Mode B and Mode AB, and Mode C defects are shown in Fig. 3(c) and (d), respectively. The estimated SL factor values for the defects of Mode A, Mode C, Mode AB, and Mode B shown in Fig. 3 are 1, 1, 3.3, and 10, respectively.

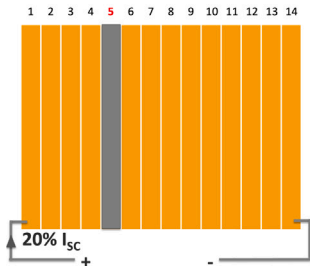
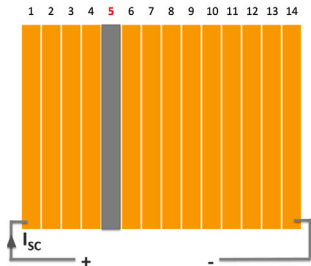
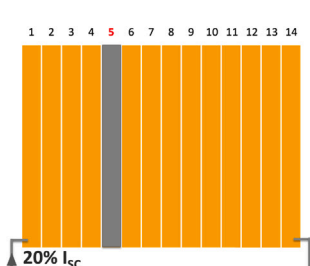
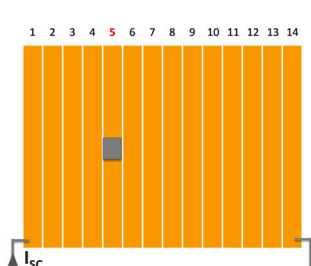
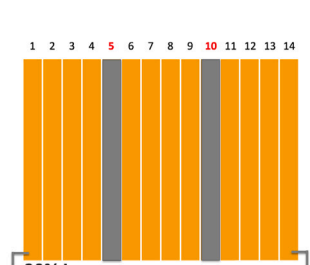
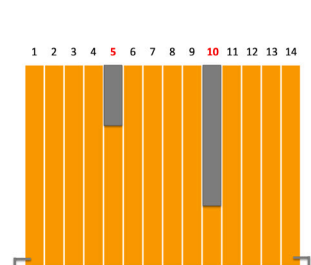
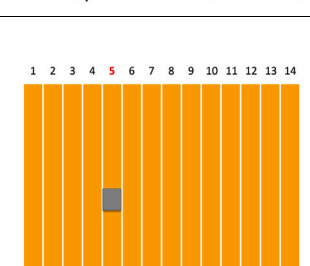
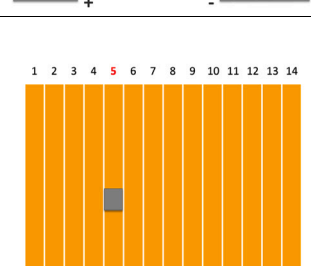
3.2. Hotspot endurance testing results

The hotspot formation in solar cells with predictor defects is analysed by capturing IR images immediately after 60 min of HSET without

removing the shading mask and ammeter connections used to short-circuit the PV panels. Representative IR images of PV modules without and with a hotspot are shown in Fig. 4(a) and (b), respectively. The opaque mask used for shading can be seen in both IR images. The average recorded temperature of the module is around 60°C. More importantly, in Fig. 4(b), a clear localized hotspot, highlighted by a white circle can be identified with reference to the background at the bottom of the shaded solar cells. Similar IR images are captured for every PV module with a predictor defect shaded together with an adjacent cell. In addition, after each round of HSET, the shaded area of the PV modules is visually inspected for any additional burn marks or discoloration. These IR images and visual inspection photographs generate the predictor-to-hotspot-to-visual defect mapping shown in Fig. 5.

Among the series of selected defective modules with divergent EL signals, Mode B defect had the highest count of 20, while Mode A had the lowest with only 4. Mode AB and Mode C defects were 10 and 13, respectively. Along with these predictor defects, 16 pairs of solar cells without any of these predictor defects are also tested for hotspots as a reference. As summarized in Table 2 and Fig. 5, shading the cells without any predictor defects does not lead to hotspots in the IR images, substantiating that defects are essential for the formation of distinguishable hotspots. The shading of low SL factor defects, such as Mode A and Mode C, also did not result in hotspots. It can be seen that Mode A defects are beneficial against localized hotspot heating as they evenly distribute the reverse current and heat across the cell area. Mode C defects are classified as mild shunts on the basis of low-injection EL imaging and do not produce strong localized hotspots because they are not strong enough to sink significant currents. In contrast, HSET of Mode B defects with the highest value of SL factor among other modes always turned into clear hotspots in IR images. All the 20 Mode B defects turned into a clearly distinguishable hotspot in the HSET and

Table 1
Summary of different modes of defects defined based on the luminescence at low-injection and high-injection EL imaging.

Mode	Low-Injection	High-injection	SL factor	Characteristics
A			~1	Severe & distributed
B			>4	Severe & local
AB			1 < SL < 4	Severe, Neither local & nor distributed
C			~1	Not severe & local

one of the hotspots formed from a Mode B defects has also resulted in discolouration of the top polymer frontsheet, corresponding to a failure following IEC61215 testing protocols. These results indicate that defects that are severe and localized (have a high SL factor) are the potential hotspots during shading. In contrast, Mode AB defects did not show a direct correlation with hotspot formation, resulting in 60% of conversion. Since the SL factor associated with Mode AB defects can vary over a range between 1 to 4, they were further classified into three groups. The first group of Mode AB defects has an SL factor of <1.5, and both the Mode AB defects under this group did not result in hotspot generation. In contrast, the group of Mode AB defects that have SL factor >3 has always turned into a hotspot during shading. This further confirms that strong localized defects are most likely to form hotspots during shading.

Further, Fig. 6 represents the IR images after HSET of the PV module shown in Fig. 3. Fig. 6(a), (b), (c), and (d) correspond to the IR images

Table 2
Summary describing the total number of predictors tested, number of hotspots formed and visual defects created due to hotspot heating for each modes of defects.

Type	No. of defects tested	No. of hotspots formed	No. of visual defect formed
Mode A	4	0	0
Mode B	20	20	1
Mode C	13	0	0
Mode AB	10	6	0
No predictor	16	0	0

taken by shading cell 5 and 6 (cell 6 had a Mode A defect), 11 and 12 (cell 12 had a Mode AB defect at the bottom area), 14 and 15 (cell 14 had a Mode B defect at the bottom) and 27 and 28 (cell 28 had a Mode

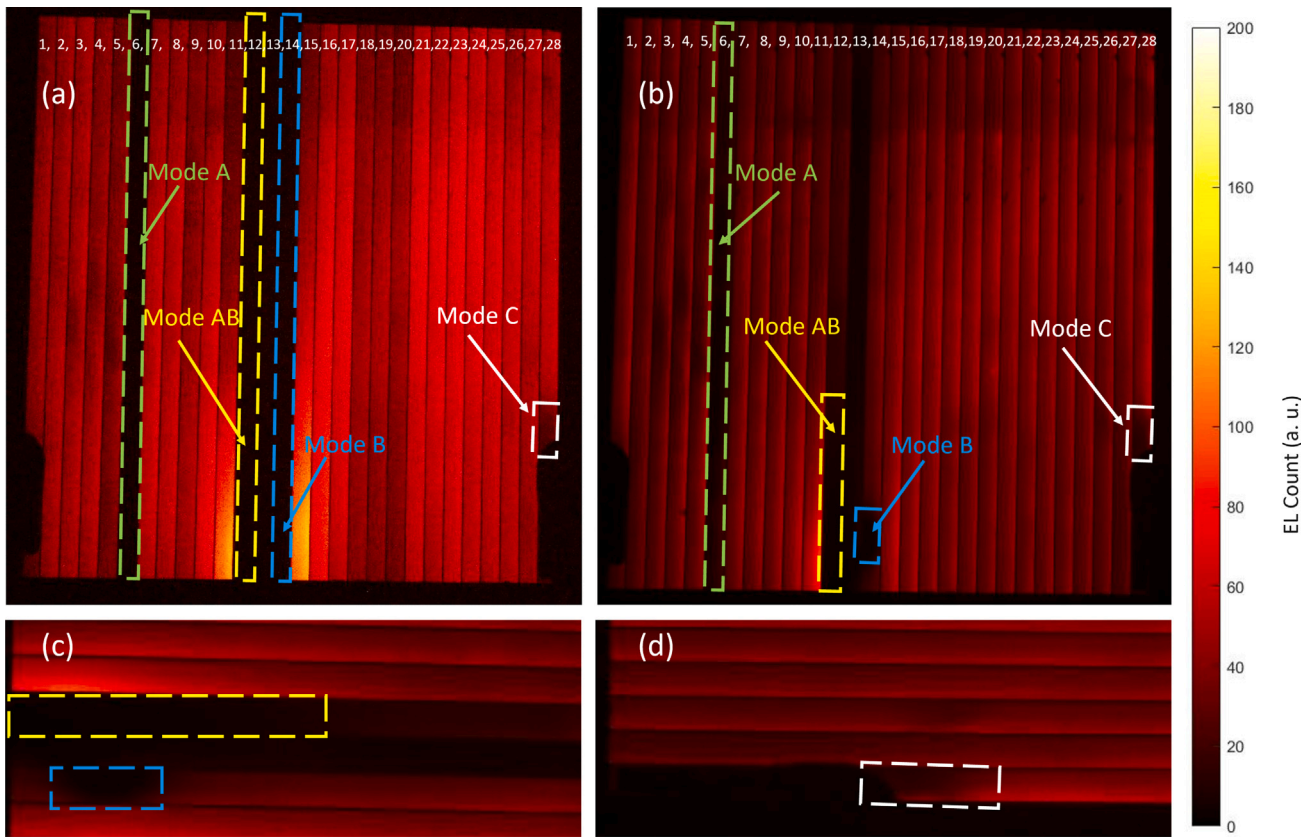


Fig. 3. EL images of a representative thin-film a-Si PV module captured at (a) low-injection and (b) high-injection. The EL signatures of Mode A, Mode B, Mode AB and Mode C defects at both low- and high-injection conditions are indicated using green, blue, yellow, and white boxes and arrows, respectively. (c) and (d) are the magnified high-injection EL images depicting the signature of Mode B (inside blue box) and Mode AB (inside yellow box), and Mode C (white) defects, respectively.

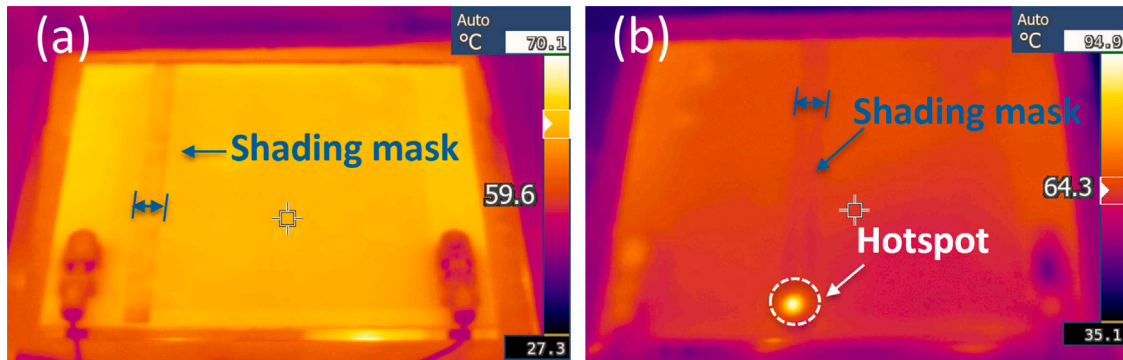


Fig. 4. IR images of thin film silicon PV module (a) without any hotspots and (b) with localized hotspots at the bottom of shaded cells. The width of shading mask is indicated using blue arrow in both the IR images and the hotspot is highlighted by a white circle in Fig. 4(b).

C defect), respectively. In agreement with previous results, the Mode A and Mode C defects did not lead to any distinguishable hotspots. Notably, both Mode AB (SL factor of 3.3) and Mode B (SL factor of 10) have transformed into a notable hotspot at the locations where the EL predictor defects were initially present. It should be noted that the Mode AB defects, in this case, have resulted in a localized or pointed hotspot irrespective of the defect exhibiting low luminescence, nearly about 30% of the cell area. More importantly, the hotspot in Fig. 6(c) is more severe than the one in Fig. 6(b), indicating that defects with a higher SL factor result in stronger hotspots in reference to relatively low SL factor defects. In the series of HSET conducted in this work, the hotspots formed from a Mode B defect in a PV module were generally more severe than those formed from a Mode AB defect. Also, the Mode

B defects that have resulted in visual defects had a SL factor close to 10. These results confirm that injection-dependent EL imaging successfully screens the defects responsible for hotspot formation in monolithic interconnected PV panels, and the SL factor extracted from high- and low-injection EL images is a clear indicator of the severity of hotspots formed from the defect.

3.3. Outlook and broader application

This work presented a method for classifying defects to screen potential hotspots in single-junction a-Si modules. However, the proposed method can be applied to any other thin-film technologies, such as cadmium telluride (CdTe), copper indium gallium selenide (CIGS),

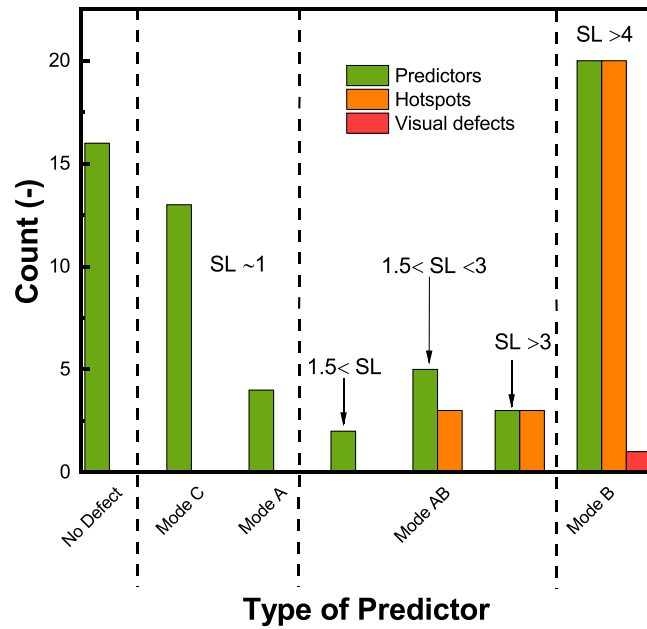


Fig. 5. Summary of HSET describing the predictor to hotspot to visual defect mapping. It is clearly seen that the higher SL factor defects, such as Mode B, always form localized hotspots, and low SL defects, such as Mode A and Mode C, do not form any hotspot during shading.

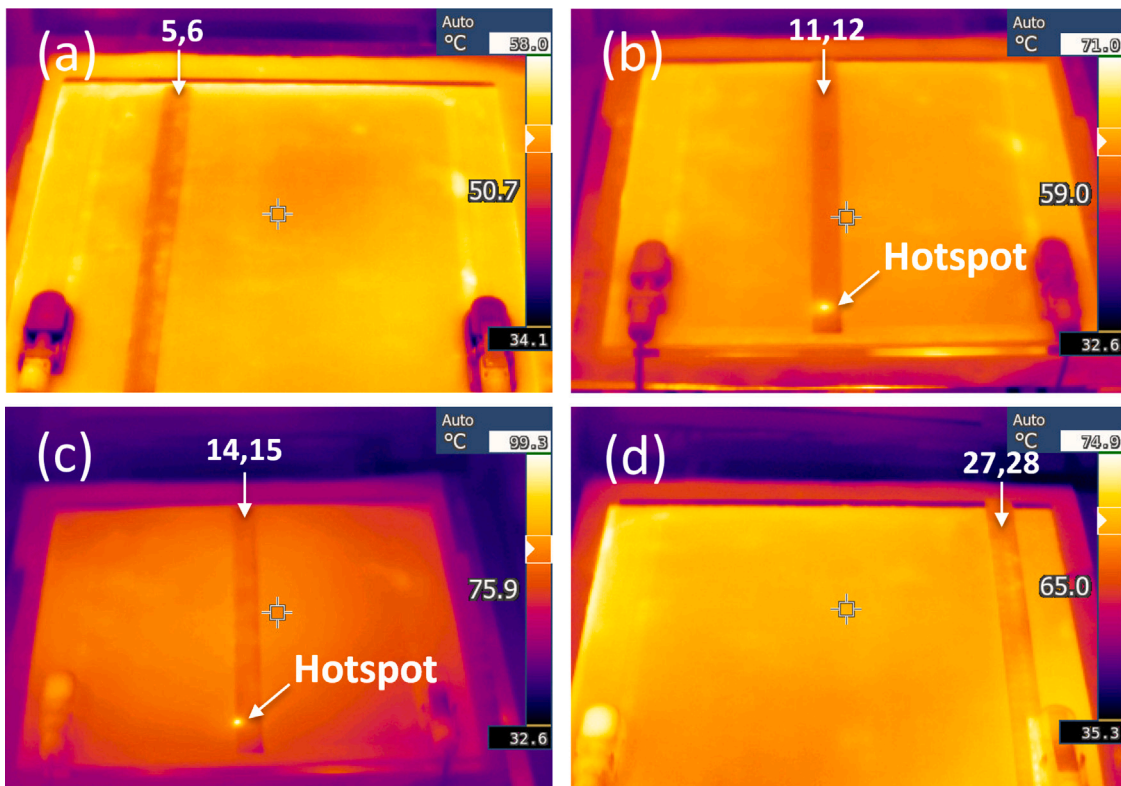


Fig. 6. IR images of thin film silicon PV modules shaded for a combination of cells with (a) Mode A, (b) Mode AB, (c) Mode B, and (d) Mode C. Mode A and Mode C defects do not turn to hotspots and Mode B and Mode AB defects formed hotspots.

organic (OPV), gallium arsenide (GaAs) and perovskites that employ monolithic interconnection for module production. This technique will be more handy for roll-to-roll produced PV panels as it can realize both localized defects that are introduced from the nonuniformity in the substrate and deposition processes, as well as the distributed defects

formed from laser scribe issues or disparity in the rolling/ milling processes.

The proposed method offers key advantages over the widely used DLIT-based approach. Firstly, unlike DLIT, injection-dependent EL imaging is a non-destructive technique, so the tested modules can

be further utilized for field installations. Moreover, classifying shunts based on severity using DLIT spatial maps is challenging due to the poor contrast of thermal images and the opaque nature of DLIT signals to certain encapsulant materials such as glass. Although the high-injection EL identifies the defects that lead to distributed shunting (Mode A defects and Mode AB defects with low SL factor), in-depth information such as the shape and areal density of defects cannot be accurately acquired by this method. A combination of DLIT and EL imaging is essential to obtain complete insight into the characteristics of the defect, such as its exact location and severity.

Although the defect definition and subsequent tests are performed on 30-cm × 28-cm area test modules, the method can also be extended to industrial PV modules of larger dimensions. However, the boundary conditions used in this work for the classification of defects need to be altered as per the cell size, as the luminescence pattern from defects may not be the same as in the test modules. For instance, in the case of long industrial PV modules, a cell may not exhibit poor luminescence across its entire area in both high- and low-injection EL imaging. Classifying defects based on the SL factor would be a universal approach for modules irrespective of their dimensions. In addition, the hotspot effects can be more severe for PV modules containing large-area cells and a higher number of interconnected cells, as they generate higher currents in reference to small-area devices and induce higher reverse bias across the cells during shading, respectively. Also, the probability of having multiple defects in a single cell increases proportionally with the increase in cell area. The presence of multiple defects, irrespective of the higher SL factor, may also bypass the localized hotspot heating effect, as these defects can evenly distribute the reverse current in the cell. Hence, defect classification and hotspot formation can be complex in the case of large-area roll-to-roll processed thin-film modules with a large areal density of defects, and future work will be to test the applicability of the proposed method and its boundary conditions on large industrial thin-film PV modules.

4. Conclusion

This study presented a method for screening the hotspots in monolithic interconnected thin-film silicon modules using EL images captured at low and high current injections. Firstly, the defects present in the modules were broadly classified as four modes based on the luminescence pattern obtained from EL images for an injected current of STC I_{SC} and 20% of STC I_{SC} . In addition, the SL factor, defined as the ratio of the fraction of the dark area of the cell at low-injection to the fraction of the dark area of the cell at high-injection, is introduced for the first time to screen the predictor defects that lead to hotspots during shading. SL factor of >4 implies that the defect is strong and localized. Defects that do not show severe shunting behaviour and defects that are distributed have relatively low SL factor values, approximately around 1. Subsequently, the classified defects are tested for their endurance to hotspot formation following the procedure discussed in IEC61215 testing norms. The HSET results suggest that defects with a high SL factor transform into strong hotspots during shading, and defects with a low SL factor of <1.5 never translate to distinguishable hotspots. In addition, it was observed that the extent of hotspot heating was directly correlated with the SL factor, i.e. higher SL factor defects form stronger hotspots. This shows that the SL factor extracted from injection-dependent EL imaging is a reliable predictor for detecting hotspot defects. The proposed method is a simple, non-destructive technique that can be applied to any thin-film technology with monolithic interconnection, and hence, is expected to gain significant attention, especially in industry settings for quality checks for roll-to-roll processed PV modules.

CRediT authorship contribution statement

K.P. Sreejith: Writing – original draft, Methodology, Formal analysis, Data curation, Conceptualization. **Niklas Zeiher:** Resources, Formal analysis, Data curation. **Peer Sluijs:** Resources, Methodology, Formal analysis. **Vijay Venkatesh:** Resources, Data curation. **Gayathri Math-iazhagan:** Supervision, Resources, Formal analysis. **Ravi Vasudevan:** Supervision, Resources, Formal analysis. **Hesan Ziar:** Writing – review & editing, Supervision. **Arno H.M. Smets:** Writing – review & editing, Supervision, Project administration, Funding acquisition.

Declaration of competing interest

The authors declare that they have no known competing financial interests or personal relationships that could have appeared to influence the work reported in this paper.

Acknowledgements

Authors from Delft University of Technology would like to thank all the students and staff members of the Thin Film Silicon Cluster of the PVMD group for their help in sample characterization. The authors also acknowledge the research and development team of HyET Solar B. V. and Dr. Subendhu Guha for useful discussions and constructive feedback. This work was supported through the TU Delft- HyET Solar bilateral contract.

Data availability

Data will be made available on request.

References

- [1] International Energy Agency, Executive summary renewables, 2024, URL <https://www.iea.org/reports/renewables-2022/executive-summary>. (Accessed on 15 March 2025).
- [2] R. Herrero, L. Olivieri, M. Victoria, R. Núñez, Integrated photovoltaics, in: *Fundamentals of Solar Cells and Photovoltaic Systems Engineering*, Elsevier, 2025, pp. 365–400.
- [3] W. Gu, S. Li, X. Liu, Z. Chen, X. Zhang, T. Ma, Experimental investigation of the bifacial photovoltaic module under real conditions, *Renew. Energy* 173 (2021) 1111–1122.
- [4] K. Sreejith, T.J. Nath, A. Kottantharayil, Comprehensive cell to module optical loss analysis of metal assisted chemically etched inverted pyramid textured multi-crystalline silicon solar cells and modules by ray-tracing method, *Sol. Energy* 244 (2022) 315–321.
- [5] R.O. Yakubu, L.D. Mensah, D.A. Quansah, M.S. Adaramola, A systematic literature review of the bifacial photovoltaic module and its applications, *J. Eng.* 2024 (8) (2024) e12421.
- [6] F. Ferroni, R.J. Hopkirk, Energy return on energy invested (EROEI) for photovoltaic solar systems in regions of moderate insolation, *Energy Policy* 94 (2016) 336–344.
- [7] A.C. Martins, V. Chapuis, A. Virtuani, C. Ballif, Robust glass-free lightweight photovoltaic modules with improved resistance to mechanical loads and impact, *IEEE J. Photovolt.* 9 (1) (2018) 245–251.
- [8] K. Jäger, J. Lensen, P. Veltman, E. Hamers, Large-area production of highly efficient flexible light-weight thin-film silicon PV modules, in: *Proc. 28th European Photovoltaic Solar Energy Conf., Paris, France, 2013*, pp. 2164–2169.
- [9] K. Sreejith, V. Venkatesh, G. Padmakumar, A.H. Smets, Comprehensive glare hazard analysis of ethylene tetrafluoroethylene (ETFE) based frontsheet for flexible photovoltaic applications, *IEEE J. Photovolt.* 14 (6) (2024) 930–936.
- [10] K. Sreejith, V. Venkatesh, P. Sluijs, K. Saleh, R. Vasudevan, A. Smets, Evaluation of glare hazard potential of flexible polymer sheet and glass encapsulant using angular intensity distribution measurements, in: *2024 IEEE 52nd Photovoltaic Specialist Conference, PVSC, IEEE, 2024*, p. 1370.
- [11] S. Dongaonkar, J.D. Servaites, G.M. Ford, S. Loser, J. Moore, R.M. Gelfand, H. Mohseni, H.W. Hillhouse, R. Agrawal, M.A. Ratner, et al., Universality of non-ohmic shunt leakage in thin-film solar cells, *J. Appl. Phys.* 108 (12) (2010).
- [12] B. Mistic, B.E. Pieters, U. Schweitzer, A. Gerber, U. Rau, Defect diagnostics of scribing failures and Cu-Rich debris in Cu (In, Ga) Se₂ thin-film solar modules with electroluminescence and thermography, *IEEE J. Photovolt.* 5 (4) (2015) 1179–1187.

- [13] Q. Zhang, Q. Li, Temperature and reverse voltage across a partially shaded Si PV cell under hot spot test condition, in: 2012 38th IEEE Photovoltaic Specialists Conference, IEEE, 2012, pp. 001344–001347.
- [14] M. Dhimish, V. Holmes, P. Mather, M. Sibley, Novel hot spot mitigation technique to enhance photovoltaic solar panels output power performance, *Sol. Energy Mater. Sol. Cells* 179 (2018) 72–79.
- [15] G. Goudelis, P.I. Lazaridis, M. Dhimish, A review of models for photovoltaic crack and hotspot prediction, *Energies* 15 (12) (2022) 4303.
- [16] M. Simon, E.L. Meyer, Detection and analysis of hot-spot formation in solar cells, *Sol. Energy Mater. Sol. Cells* 94 (2) (2010) 106–113.
- [17] S. Daliento, F. Di Napoli, P. Guerriero, V. d'Alessandro, A modified bypass circuit for improved hot spot reliability of solar panels subject to partial shading, *Sol. Energy* 134 (2016) 211–218.
- [18] P. Manganiello, M. Balato, M. Vitelli, A survey on mismatching and aging of PV modules: The closed loop, *IEEE Trans. Ind. Electron.* 62 (11) (2015) 7276–7286.
- [19] H. Hanifi, M. Pander, B. Jaeckel, J. Schneider, A. Bakhtiari, W. Maier, A novel electrical approach to protect PV modules under various partial shading situations, *Sol. Energy* 193 (2019) 814–819.
- [20] W. Herrmann, W. Wiesner, W. Vaassen, Hot spot investigations on PV modules—new concepts for a test standard and consequences for module design with respect to bypass diodes, in: Conference Record of the Twenty Sixth IEEE Photovoltaic Specialists Conference-1997, IEEE, 1997, pp. 1129–1132.
- [21] F. Fertig, S. Rein, M. Schubert, W. Warta, Impact of junction breakdown in multicrystalline silicon solar cells on hot spot formation and module performance, *Cell* 40 (2011) 1–26.
- [22] I. Geisemeyer, F. Fertig, W. Warta, S. Rein, M.C. Schubert, Impact of reverse breakdown in shaded silicon solar cells on module level: simulation and experiment, in: European Photovoltaic Solar Energy Conference and Exhibition (EU PVSEC) 2012, 2012.
- [23] O. Breitenstein, J. Bauer, K. Bothe, W. Kwapil, D. Lausch, U. Rau, J. Schmidt, M. Schneemann, M.C. Schubert, J.-M. Wagner, et al., Understanding junction breakdown in multicrystalline solar cells, *J. Appl. Phys.* 109 (7) (2011).
- [24] D.C. Jordan, T.J. Silverman, J.H. Wohlgemuth, S.R. Kurtz, K.T. VanSant, Photovoltaic failure and degradation modes, *Prog. Photovolt., Res. Appl.* 25 (4) (2017) 318–326.
- [25] M.A. Garcia, W. Herrmann, W. Böhrer, B. Proisy, Thermal and electrical effects caused by outdoor hot-spot testing in associations of photovoltaic cells, *Prog. Photovolt., Res. Appl.* 11 (5) (2003) 293–307.
- [26] S.W. Ko, Y.C. Ju, H.M. Hwang, J.H. So, Y.-S. Jung, H.-J. Song, H.-e. Song, S.-H. Kim, G.H. Kang, Electric and thermal characteristics of photovoltaic modules under partial shading and with a damaged bypass diode, *Energy* 128 (2017) 232–243.
- [27] P. Guerriero, P. Tricoli, S. Daliento, A bypass circuit for avoiding the hot spot in PV modules, *Sol. Energy* 181 (2019) 430–438.
- [28] R.G. Vieira, F.M. de Araújo, M. Dhimish, M.I. Guerra, A comprehensive review on bypass diode application on photovoltaic modules, *Energies* 13 (10) (2020) 2472.
- [29] S. Ahsan, K.A.K. Niazi, H.A. Khan, Y. Yang, Hotspots and performance evaluation of crystalline-silicon and thin-film photovoltaic modules, *Microelectron. Reliab.* 88 (2018) 1014–1018.
- [30] S. Dongaonkar, M.A. Alam, Geometrical design of thin film photovoltaic modules for improved shade tolerance and performance, *Prog. Photovolt., Res. Appl.* 23 (2) (2015) 170–181.
- [31] C. Tzikas, G. Gómez, M. van den Donker, K. Bakker, A. Smets, W. Folkerts, Do thin film PV modules offer an advantage under partial shading conditions, in: Proceedings of the 33rd European Photovoltaic Solar Energy Conference and Exhibition, Amsterdam, the Netherlands, 2017, pp. 25–29.
- [32] T.D. Lee, A.U. Ebong, A review of thin film solar cell technologies and challenges, *Renew. Sustain. Energy Rev.* 70 (2017) 1286–1297.
- [33] S. Dongaonkar, C. Deline, M.A. Alam, Performance and reliability implications of two-dimensional shading in monolithic thin-film photovoltaic modules, *IEEE J. Photovolt.* 3 (4) (2013) 1367–1375.
- [34] Terrestrial Photovoltaic (PV) Modules – Design Qualification and Type Approval – Part 1-3: Special Requirements for Testing of Thin-Film Amorphous Silicon Based Photovoltaic (PV) Modules, Standard, Vol. 2005, International Electrotechnical Commission, Geneva, CH, 2005.
- [35] M. Alonso-García, J. Ruiz, F. Chenlo, Experimental study of mismatch and shading effects in the I–V characteristic of a photovoltaic module, *Sol. Energy Mater. Sol. Cells* 90 (3) (2006) 329–340.
- [36] Y. Chen, X. Wang, D. Li, R. Hong, H. Shen, Parameters extraction from commercial solar cells I–V characteristics and shunt analysis, *Appl. Energy* 88 (6) (2011) 2239–2244.
- [37] K. Bouzidi, M. Chegaar, A. Bouhemadou, Solar cells parameters evaluation considering the series and shunt resistance, *Sol. Energy Mater. Sol. Cells* 91 (18) (2007) 1647–1651.
- [38] M.U. Ali, H.F. Khan, M. Masud, K.D. Kallu, A. Zafar, A machine learning framework to identify the hotspot in photovoltaic module using infrared thermography, *Sol. Energy* 208 (2020) 643–651.
- [39] E. Molenbroek, D. Waddington, K. Emery, Hot spot susceptibility and testing of PV modules, in: Photovoltaic Specialists Conference, Vol. 1, Las Vegas, 1991, pp. 547–552.
- [40] Z.A. Jaffery, A.K. Dubey, A. Haque, et al., Scheme for predictive fault diagnosis in photo-voltaic modules using thermal imaging, *Infrared Phys. Technol.* 83 (2017) 182–187.
- [41] H. Liu, C. Zhang, D. Huang, Extreme learning machine and moving least square regression based solar panel vision inspection, *J. Electr. Comput. Eng.* 2017 (1) (2017) 7406568.
- [42] O. Breitenstein, J. Bauer, K. Bothe, D. Hinken, J. Müller, W. Kwapil, M.C. Schubert, W. Warta, Can luminescence imaging replace lock-in thermography on solar cells? *IEEE J. Photovolt.* 1 (2) (2011) 159–167.
- [43] O. Breitenstein, J. Bauer, T. Trupke, R.A. Bardos, On the detection of shunts in silicon solar cells by photo-and electroluminescence imaging, *Prog. Photovolt., Res. Appl.* 16 (4) (2008) 325–330.
- [44] H. Straube, O. Breitenstein, Infrared lock-in thermography through glass substrates, *Sol. Energy Mater. Sol. Cells* 95 (10) (2011) 2768–2771.
- [45] S. Roy, R. Gupta, Quantitative estimation of shunt resistance in crystalline silicon photovoltaic modules by electroluminescence imaging, *IEEE J. Photovolt.* 9 (6) (2019) 1741–1747.
- [46] V.E. Puranik, R. Kumar, R. Gupta, Progress in module level quantitative electroluminescence imaging of crystalline silicon PV module: A review, *Sol. Energy* 264 (2023) 111994.
- [47] S. Deitsch, V. Christlein, S. Berger, C. Buerhop-Lutz, A. Maier, F. Gallwitz, C. Riess, Automatic classification of defective photovoltaic module cells in electroluminescence images, *Sol. Energy* 185 (2019) 455–468.
- [48] B. Doll, K. Forberich, J. Hepp, S. Langner, C. Buerhop-Lutz, J.A. Hauch, C.J. Brabec, I.M. Peters, Luminescence analysis of PV-module soiling in Germany, *IEEE J. Photovolt.* 12 (1) (2021) 81–87.
- [49] A.S. Rajput, J.W. Ho, Y. Zhang, S. Nalluri, A.G. Aberle, Quantitative estimation of electrical performance parameters of individual solar cells in silicon photovoltaic modules using electroluminescence imaging, *Sol. Energy* 173 (2018) 201–208.
- [50] A.S. Rajput, Y. Zhang, C.D. Rodriguez-Gallegos, A. Khanna, P.K. Basu, S. Nalluri, J.P. Singh, Comparative study of the electrical parameters of individual solar cells in a c-Si module extracted using indoor and outdoor electroluminescence imaging, *IEEE J. Photovolt.* 10 (5) (2020) 1396–1402.
- [51] A.M. Karimi, J.S. Fada, N.A. Parrilla, B.G. Pierce, M. Koyutürk, R.H. French, J.L. Braid, Generalized and mechanistic PV module performance prediction from computer vision and machine learning on electroluminescence images, *IEEE J. Photovolt.* 10 (3) (2020) 878–887.
- [52] T. Kropp, M. Schubert, J.H. Werner, Quantitative prediction of power loss for damaged photovoltaic modules using electroluminescence, *Energies* 11 (5) (2018) 1172.
- [53] V.E. Puranik, R. Gupta, Standardized applications of electroluminescence imaging for efficient investigation of potential-induced degradation shunting in crystalline silicon photovoltaic module, *Sol. Energy* 245 (2022) 183–192.
- [54] Y. Wang, L. Li, Y. Sun, J. Xu, Y. Jia, J. Hong, X. Hu, G. Weng, X. Luo, S. Chen, et al., Adaptive automatic solar cell defect detection and classification based on absolute electroluminescence imaging, *Energy* 229 (2021) 120606.
- [55] U. Rau, V. Huhn, B.E. Pieters, Luminescence analysis of charge-carrier separation and internal series-resistance losses in Cu (In, Ga) Se 2 solar cells, *Phys. Rev. Appl.* 14 (1) (2020) 014046.
- [56] S. Villa, R. Aninat, P. Yilmaz, A. Kingma, M. Dziechciarz, J. van den Berg, K. Bakker, M. Theelen, Insights into the moisture-induced degradation mechanisms on field-deployed CIGS modules, *Prog. Photovolt., Res. Appl.* 31 (8) (2023) 824–839.
- [57] A. Gerber, V. Huhn, T. Tran, M. Siegloch, Y. Augarten, B. Pieters, U. Rau, Advanced large area characterization of thin-film solar modules by electroluminescence and thermography imaging techniques, *Sol. Energy Mater. Sol. Cells* 135 (2015) 35–42.
- [58] A. Helbig, T. Kirchartz, R. Schaeffler, J.H. Werner, U. Rau, Quantitative electroluminescence analysis of resistive losses in Cu (In, Ga) Se2 thin-film modules, *Sol. Energy Mater. Sol. Cells* 94 (6) (2010) 979–984.
- [59] M. Diethelm, L. Penninck, M. Regnat, T. Offermans, B. Zimmermann, C. Kirsch, R. Hiestand, S. Altazin, B. Ruhstaller, Finite element modeling for analysis of electroluminescence and infrared images of thin-film solar cells, *Sol. Energy* 209 (2020) 186–193.
- [60] K. Ramspeck, K. Bothe, D. Hinken, B. Fischer, J. Schmidt, R. Brendel, Recombination current and series resistance imaging of solar cells by combined luminescence and lock-in thermography, *Appl. Phys. Lett.* 90 (15) (2007).
- [61] T. Fuyuki, H. Kondo, Y. Kaji, A. Ogane, Y. Takahashi, Analytic findings in the electroluminescence characterization of crystalline silicon solar cells, *J. Appl. Phys.* 101 (2) (2007).
- [62] V.E. Puranik, R. Gupta, Analysis and insight of electroluminescence imaging in the assessment of potential-induced degradation in crystalline silicon photovoltaic module, *Eng. Fail. Anal.* 134 (2022) 106027.
- [63] F. Li, D.J. Colvin, V.S.P. Buddha, K.O. Davis, G. Tamizhmani, Electroluminescence and infrared imaging of fielded photovoltaic modules: A complementary analysis of series resistance-related defects, *Sol. Energy* 276 (2024) 112704.
- [64] M. Liggett, D.J. Colvin, A. Ballen, M. Matam, H.P. Seigneur, M. Li, A.M. Gabor, P.J. Knodle, C.J. Neal, S. Seal, et al., Characterization of field-exposed photovoltaic modules featuring signs of contact degradation, *IEEE J. Photovolt.* (2025).